International Journal of Applied Mechanics
Vol. 6, No. 6 (2014) 1450067 (28 pages)

DOI: 10.1142/S1758825114500677

Imperial College Press
www.icpress.co.uk

UNCERTAINTY ANALYSIS OF A ONE-DIMENSIONAL CONSTITUTIVE MODEL FOR SHAPE MEMORY ALLOY THERMOMECHANICAL DESCRIPTION

SERGIO A. OLIVEIRA

Department of Mechanical Engineering
Centro Federal de Educação Tecnológica Celso Suckow da Fonseca
20.271.110 Rio de Janeiro, RJ, Brazil
amserol@yahoo.com.br

MARCELO A. SAVI

COPPE — Department of Mechanical Engineering
Universidade Federal do Rio de Janeiro
P. O. Box 68.503, 21.941.972 Rio de Janeiro, RJ, Brazil
savi@mecanica.ufrj.br

ILMAR F. SANTOS

Department of Mechanical Engineering
Technical University of Denmark
2800 Kongens Lyngby, Denmark
ifs@mek.dtu.dk

Received 21 November 2013
Revised 15 September 2014
Accepted 12 October 2014
Published 27 November 2014

The use of shape memory alloys (SMAs) in engineering applications has increased the interest of the accuracy analysis of their thermomechanical description. This work presents an uncertainty analysis related to experimental tensile tests conducted with shape memory alloy wires. Experimental data are compared with numerical simulations obtained from a constitutive model with internal constraints employed to describe the thermomechanical behavior of SMAs. The idea is to evaluate if the numerical simulations are within the uncertainty range of the experimental data. Parametric analysis is also developed showing the most sensitive constitutive parameters that contribute to the uncertainty. This analysis provides the contribution of each parameter establishing the accuracy of the constitutive equations.

Keywords: Shape memory alloys; smart materials; constitutive model; uncertainty; experimental.

1. Introduction

Shape memory alloys (SMAs) have a thermomechanical behavior that provides a wide range of applications in different fields of knowledge. The thermomechanical

behavior of these alloys is associated with thermoelastic martensitic phase transformations that are responsible for the unique characteristics of these smart materials. Literature presents several articles that investigate the SMA thermomechanical behavior, discussing distinct aspects of modeling, simulation and experimental approaches.

In brief, it is possible to say that SMA thermomechanical behavior is very complex due to the coupling of several phenomena, presenting hysteretic response. Pseudoelastic and shape memory effects are the most important behaviors in terms of SMA applicability. Nevertheless, the general behavior has other important aspects that need to be understood properly in order to define SMA applications. Transformation induced plasticity is one of these aspects that imposes a previous training process to SMA devices before their use in a specific application.

Lagoudas [2008] and Paiva and Savi [2006] presented a general overview of SMA applications especially in engineering field. Self-expanded structures, multi-actuated structures and robotics are some possibilities that are exploiting SMA characteristics. Machado and Savi [2003] discussed SMA biomedical devices that are usually employed in surgical instruments, cardio-vascular, orthopedic and orthodontic devices, among other possibilities. Self-expansive structures constitute one of the main applications of SMAs, as the Simon filters and stents. Czechowicz [2013] presented an overview of automotive applications related to SMAs. An overview about dynamical applications involving systems with SMA elements was discussed in Savi [2014]. Basically, dynamical applications try to exploit both the adaptive dissipation associated with hysteretic behavior and changes in mechanical properties caused by phase transformations.

Due to the complex thermomechanical behavior of SMAs, several researches are dedicated to investigate a proper SMA description. The three-dimensional (3D) description is even more complex, involving difficulties introduced either by the modeling or by experimental analyses related to multiaxial tests. The constitutive modeling of SMAs is based on macroscopic features of their thermomechancial behavior. Lagoudas [2008] and Paiva and Savi [2006] presented a general overview of these efforts, highlighting phenomenological constitutive models for SMAs. Concerning recent reports, it is important to highlight 3D modeling efforts: Auricchio *et al.* [2014], Mehrabi *et al.* [2014], Andani and Elahinia [2014], Andani *et al.* [2013], Chapman *et al.* [2011], Lagoudas *et al.* [2011] and Panico and Brinson [2007].

Paiva *et al.* (2005) developed a one-dimensional (1D) constitutive model based on the Fremond theory [Fremond, 1996], within the scope of standard generalized materials [Lemaitre and Chaboche, 1990]. Oliveira *et al.* [2010] treated a 3D extension of a simplified version of this model. Several references discussed the main aspects of this model. Among them, it is important to highlight the following references: Savi *et al.* [2002], Baêta Neves *et al.* [2004], Paiva *et al.* [2005], Savi and Paiva [2005] and Aguiar *et al.* [2010].

Mathematical models are usually employed to describe a physical phenomenon and it is expected that they produce similar results compared with experimental tests. Nevertheless, deviations between experimental data and theoretical results are common. This discrepancy may be related to uncertainty issues associated with experimental measurements and their calculations provide a better comparison between numerical and experimental results. This analysis increases the possibility of numerical results to be within a proper range.

In this regard, it is important to observe that inaccuracies are unavoidable in experimental tests being related to different sources and magnitudes of systematic and random errors that can influence the measurements. Therefore, it is important to investigate the main aspects about them evaluating the uncertainty associated with experimental data. This approach allows one to establish a proper comparison between numerical and experimental data. Moffat [1985, 1988], Coleman and Steele [1995], Steele and Coleman [1987] and Barbato *et al.* [2005] presented a description of the sources of errors in engineering measurements and the relationship between errors and uncertainties.

This work presents an uncertainty analysis related to experimental tensile tests conducted with SMA wires. Features of the tensile equipment are evaluated for the uncertainty calculation. Under this assumption, it is defined a range around experimental data imposed by the uncertainties. Experimental data are compared with numerical simulations obtained from the constitutive model proposed by Paiva *et al.* [2005] to describe the thermomechanical behavior of SMAs. The idea is to evaluate if the numerical simulations are within the uncertainty range of the experimental data. Parametric analysis is also developed showing the most sensitive constitutive parameters that contribute to the uncertainty.

2. Experimental Test

SMA characterization is associated with several experimental tests including tensile and digital scanning calorimeter (DSC) tests. The first one establishes the general thermomechanical behavior while the second defines the phase transformation temperatures. SMA wires are in focus and ASTM F2063 is employed to guide the tests. It is assumed that only tensile tests contribute to uncertainty analysis since it defines the main features related to the thermomechanical behavior of SMAs.

2.1. *Tensile tests*

This subsection deals with tensile tests performed with SMA wires. Ni-Ti wires with a circular cross section of 0.853 mm diameter, manufactured by Dynalloy Inc., are of concern. A universal testing system "INSTRON 6022" is employed with a 10 kN load cell. Tests are conducted considering a prescribed strain loading with a ratio of 0.205/s and a maximum force of 200 N that provides strains within the yield surface. The equipment is connected to a computer that controls the test details

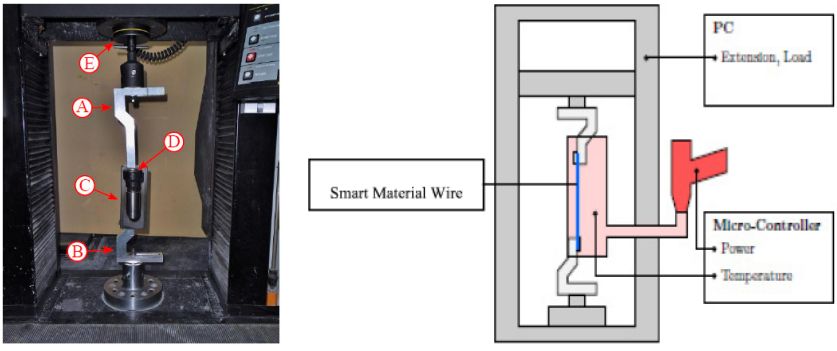

(a) (b)

Fig. 1. (Color online) (a) Test-rig for tension test of SMA wires. The upper grip (A) and lower grip (B) hold the SMA wire, which is inside the oven (C). The air inlet from a heat gun for the oven is (D). Forces are measured by a 10 KN load cell. (b) Schematics of test-rig used for tension tests of SMA wires (blue) at different constant temperatures controlled with use of a heat gun (red). The grips (light gray) are attached to the INSTRON testing system (dark gray).

and records experimental data. A device assembled with a heat gun promotes air inflation employed for temperature control. Figure 1 shows the experimental test apparatus.

Tensile tests are performed at different temperatures and all specimens are subjected to a proper training process. Initially, the SMA specimen is trained by assuming a temperature $T = 303\,\mathrm{K}$, and being subjected to 50 mechanical cycles. Figure 2(a) shows stress–strain curves of this training procedure. Note that SMA response has an asymptotic behavior converging to a hysteresis loop. After this training process, the wire is heated to a temperature of 373 K and cooled down to

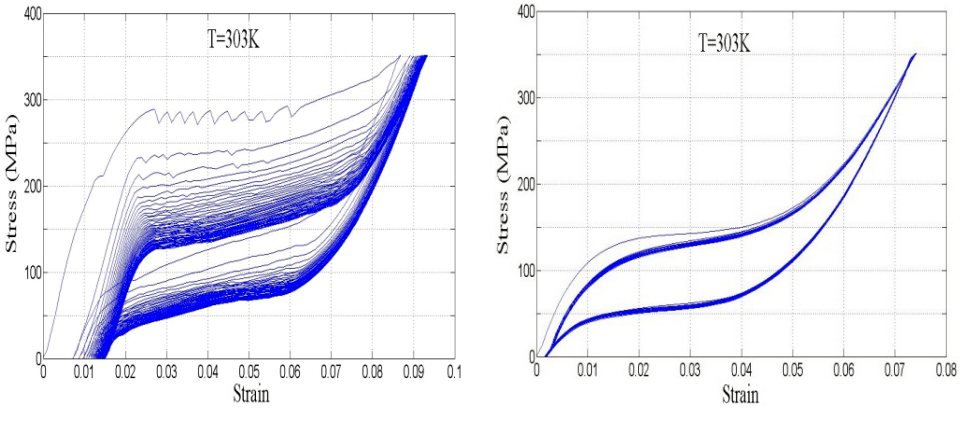

(a) (b)

Fig. 2. Pseudoelastic test. (a) Training process of 50 cycles. (b) Pseudoelastic test of 20 cycles using the trained specimen.

a temperature of 303 K and afterward, a 20 cycles test is carried out. Figure 2(b) shows the stress–strain curve of the trained specimen.

This result illustrates the classical pseudoelastic effect characterized by the hysteresis loop. In brief, the SMA sample presents a linear elastic response until a critical stress value is reached. After this point, austenite–martensite phase transformation starts. When this phase transformation finishes, the SMA presents a linear elastic response in the martensitic phase. During the unloading, the sample presents a linear response until the critical stress value for reverse transformation is reached. Afterward, martensite–austenite phase transformation starts. At the end of this phase transformation, linear elastic response occurs again. When the load is completely removed, the sample returns to the original configuration. Nevertheless, it is important to note that the irreversibility of the process is related to the dissipation associated with the hysteresis loop.

2.2. *DSC test*

Differential Scanning Calorimeter (DSC) test has the objective to evaluate the phase transformation temperatures in SMAs. The equipment heats up and cools down the specimen in a chosen temperature range and captures the amount of thermal power needed for maintaining a specified constant temperature rate in time. The DSC test is performed with the equipment "DSC 200 F3 Maia", presented in Fig. 3(a).

DSC test is expressed by means of the heat as a function of the temperature, containing peaks at the phase transformation temperatures of the material. Exothermic or endothermic reactions are possible depending on the direction of the phase transformation. Usually, four temperatures defines the SMA behavior: T_i^M and T_f^M, respectively the temperatures where martensitic phase transformation starts and finishes; T_i^A and T_f^A, the temperatures where the austenitic phase starts and finishes. A cycle of a sequence of 11 cycles is shown in Fig. 3(b). This result defines the phase transformation temperatures that are calculated from the tangent method,

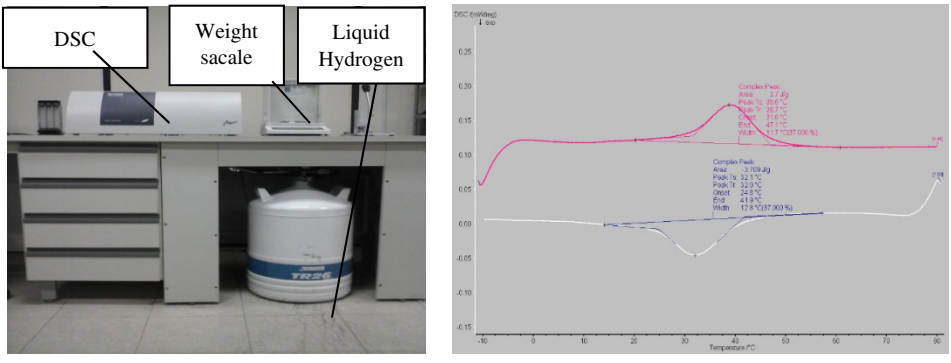

(a) (b)

Fig. 3. DSC Test. (a) DSC 200 F3 Maia. (b) Phase transformation temperatures.

Table 1. The initial and final martensite phase transformation temperatures for each cycle.

	$T_f^M(K)$	$T_i^M(K)$		$T_f^M(K)$	$T_i^M(K)$
Cycle 1	269.05	292.80	Cycle 7	269.95	293.00
Cycle 2	271.95	293.70	Cycle 8	270.45	292.70
Cycle 3	270.45	293.40	Cycle 9	269.85	292.80
Cycle 4	269.75	293.10	Cycle 10	270.85	293.30
Cycle 5	268.95	293.40	Cycle 11	269.25	291.30
Cycle 6	270.85	294.10	Average	270.12	293.30

indicated in Fig. 3(b). The tangent method is employed for the determination of the phase transformation temperatures. Table 1 presents martensitic phase transformation temperatures for each one of the eleven cycles together with their average values.

For the sake of simplicity, the uncertainties related to phase transformation temperatures evaluated from the DSC tests are neglected. The average temperature T_i^M is used for uncertainty analysis. Therefore, all uncertainties are related to the tensile tests.

3. Uncertainty Analysis

The uncertainty analysis considers tensile tests of the SMA wire at different temperatures presenting pseudoelastic behavior. The first step is to promote a filtering process, eliminating systematic errors using outlier detection technique. Afterward, constitutive model is presented defining sensitivity coefficients for each model parameter. Uncertainty contributions are then analyzed considering type A, estimated using statistical methods, and type B, evaluated according to non-statistical methods. Figure 4 shows a sequence employed by the uncertainty analysis.

3.1. *Methods for uncertainty analysis*

International organizations related to methodologies and standards published a fundamental text known as GUM [2008] (Guide to the Expression of Uncertainty in Measurement), which was incorporated into European standard ENV 13005. This reference defines two types of uncertainty contributions: type A, related to statistical methods; and type B, associated with non-statistical methods. This classification provides two different ways for uncertainty evaluation, and does not indicate a difference in the nature of these two types of evaluation. The resulting uncertainty components of each type are quantified by variance or standard deviation. In this work, uncertainties are evaluated from the constitutive model considering the influence of the parameters, the temperature T, and the number of cycles. The first two cases can be classified as type B, while the last one is of type A [Barbato *et al.*, 2005].

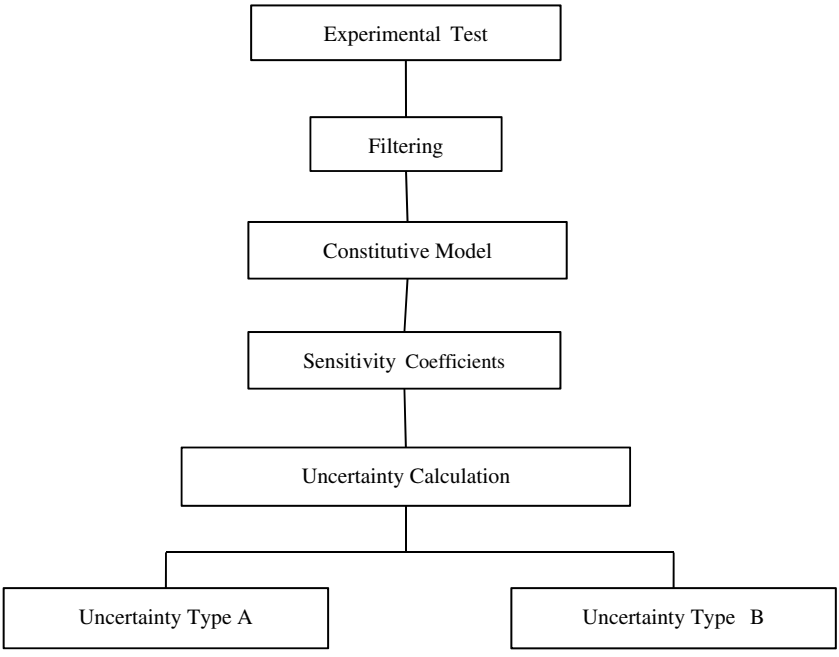

Fig. 4. Flowchart of the uncertainty analysis.

3.1.1. *Statistical methods*

The application of statistical methods can be used in filtering data in order to eliminate systematic errors. Barbato *et al.* [2005] considers the use of statistical methods as a type A analysis. Systematic effects are characterized by three factors: Constant systematic errors; variable systematic errors; and measurement accidents. The first group includes calibration errors, and may be avoided by a proper instrument calibration and measurement procedures. Variable systematic errors include the effect of large temperature variation over replicated measurements. Concerning measurement accidents, they are usually related to electromagnetic disturbances, being detected by normality tests and exclusion principles.

The detection and estimation of systematic and random errors can be done through tools such as normal and student distributions. Outlier technique can be employed to eliminate these errors. Normal distribution has less accurate values for small samples, which leads us to the use of the student distribution. Moreover, the uncertainty analysis can be performed using the standard deviation, confidence level, expanded uncertainty and degree of freedom for the analyzed data.

The correction of systematic errors is usually performed using statistical methods that promote a consistent adjustment with experimental data. In this regard, polynomial regression is widely employed for this purpose. Based on residue, r^1, defined as the difference between experimental data and the value obtained by the

regression model, it is possible to determine important variables related to uncertainty analysis: trend; standard deviation of each parameter and determination coefficient.

The determination coefficient is defined as the square of the Pearson correlation coefficient, $\mathbb{R}$, which is a measure of the degree of linear relationship between two quantitative variables. The Pearson correlation coefficient varies between -1 and $+1$. This coefficient vanishes when the adopted regression is not appropriate. Therefore, the closer the coefficient is to $+1$ or -1, the stronger is the association between two variables. The Pearson correlation coefficient is calculated according to the following expression:

$$\mathbb{R} = \frac{\sum_{i=1}^{n}(\varepsilon_i - \bar{\varepsilon})(r_i^1 - \overline{r}^1)}{\sqrt{\sum_{i=1}^{n}(\varepsilon_i - \bar{\varepsilon})^2}\sqrt{\sum_{i=1}^{n}(r_i^1 - \overline{r}^1)^2}} \tag{3.1}$$

where

$$\overline{r}^1 = \frac{1}{n}\sum_{i=1}^{n} r_i^1, \tag{3.2}$$

$$\bar{\varepsilon} = \frac{1}{n}\sum_{i=1}^{n} \varepsilon_i. \tag{3.3}$$

The Pearson correlation coefficient is interpreted as follows:

- $|\mathbb{R}| \geq 0.70$ – strong correlation.
- $0.30 \leq |\mathbb{R}| < 0.7$ – moderate correlation.
- $0 \leq |\mathbb{R}| < 0.30$ – weak correlation.

The standard deviation or standard error of the residues, s^{r^1}, is employed to indicate how the data are sparse. The number of degrees of freedom is the difference between the number of analyzed data and the number of coefficients of the polynomial chosen to perform the regression.

Outlier technique is employed by applying the Chauvenet's criterion on residue values. This criterion specifies that a measurement may be rejected if the probability of obtaining a particular deviation of the estimated average is less than $\frac{1}{4n^d}$, where n^d is the number of residues. By applying the Chauvenet's criterion to eliminate unreliable data, it is necessary to calculate the residues average, m^{r^1}, and the standard deviation of the residues, s^{r^1}, using all the obtained data. The rejected data occupy the extreme areas under the normal curve, as represented in Fig. 5. Thus, for each value of n^d it is possible to calculate the probability $(1 - \frac{1}{4n^d})$. By integrating the density function of the normal distribution it is determined the coefficient z that corresponds to the number of standard deviations of the range of acceptable values. The point is eliminated if the residue value exceeds the limits of the considered interval defined, $m^{r^1} \pm z s^{r^1}$.

The adjustment validation is another important analysis that is done considering the regression robustness. A proper validation is evaluated from the robustness

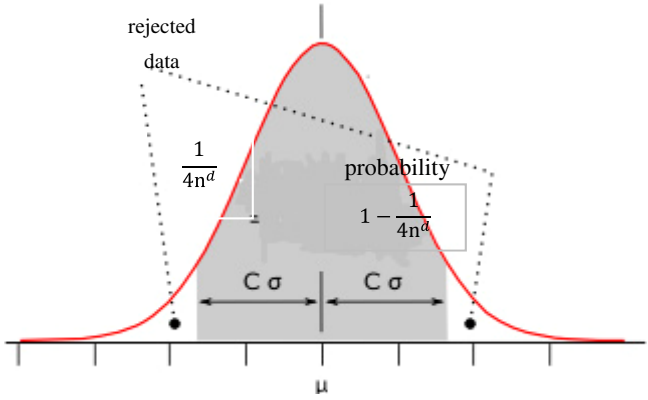

Fig. 5. Normal distribution.

index, when it has values much greater than 1. This procedure checks if the adjustment introduces significant changes when the experiment is repeated. Standard deviation of the polynomial coefficients defines a variation range, considering the corresponding confidence interval.

The uncertainty U is defined from the product of the student factor of the distribution for a given confidence level, J, and the standard deviation of the coefficients, s.

$$U = Js. \tag{3.4}$$

The degree of freedom can be classified as follows: very reliable: 100; reliable: 30; unreliable: 15. Robustness is the ratio between the coefficient and the relevant uncertainty of the coefficient. The higher is the robustness the more stable is the variation range of the coefficients.

The coefficient analysis χ^2 [chi-square] identifies systematic errors. Its calculation needs the introduction of some coefficients. First, let us define the number of classes, n^c, to define the theoretical normal distribution [Barbato *et al.*, 2005].

$$n^c = \sqrt{n^d} + z. \tag{3.5}$$

The limits of the range is defined by $m^{r^1} \pm zs^{r^1}$, where it is assumed $z = 4$. Therefore, the size of each class is calculated as follows:

$$D^c = \frac{(m^{r^1} + zs^{r^1}) - (m^{r^1} - zs^{r^1})}{n^c}. \tag{3.6}$$

Experimental absolute frequency f_a (observed frequency) is calculated from the number of times that each residue value appears at the interval for each class. The definition of the limits of each interval of the respective classes ($l1$ and $l2$), allows one to calculate the normal distribution of the average and the standard deviation of the residue for each limit value (d_n^{l1} and d_n^{l2}), respectively, and estimate the difference between them. The absolute theoretical frequency, f_{at} (expected frequency),

is calculated as:

$$f_{at} = (d_n^{l1} - d_n^{l2})n^d. \tag{3.7}$$

The experimental coefficient χ_e^2 is calculated as follows:

$$\chi_e^2 = \frac{(f_a - f_{at})^2}{f_{at}}. \tag{3.8}$$

From the experimental coefficient χ_e^2, it is possible to calculate the lower and upper bounds for the theoretical coefficient χ_T^2. The lower limit is estimated using the inverse of the probability of the chi-square distribution where the probability is given by

$$\text{Prob}^{ti} = 1 - \frac{(1 - N^c)}{2}. \tag{3.9}$$

On the other hand, the upper limit is calculated using the inverse of the probability of the chi-square distribution where the probability is calculated as follows:

$$\text{Prob}^{ts} = \frac{(1 - N^c)}{2}, \tag{3.10}$$

where N^c is the confidence level. Here, it is assumed a value of 80%. The definition of degrees of freedom for the class number (dof) is given by:

$$\text{dof} = n^c - 1 - 2, \tag{3.11}$$

where the value 1 refers to the average where the value 2 refers to the lower and upper limits of each class. In this work, it is assumed that the number of class is equal to 14 and the degree of freedom is equal to 11.

After the definition of the lower and upper bounds for the theoretical coefficient χ_T^2, it is important to check if the experimental coefficient χ_e^2 is within the range of the theoretical coefficient χ_T^2. In positive case, the data does not present systematic errors.

3.1.2. *Non-statistical methods*

The uncertainty contributions of type B are associated with non-statistical methods. The variance is estimated from available information on possible variability of measurement magnitudes. This information may include: data from previous measurements; experience or general knowledge of the behavior and properties of materials and relevant instruments manufacturer's specifications data provided in calibration's certificates and other certificates, uncertainties assigned to reference data taken from handbooks. The uncertainty calculation uses the method PUMA (Procedure for Uncertainty Management) introduced by ISO 14253-2 that allows the calculation without the knowledge of details about the uncertainties contribution.

The uncertainty analysis of type B related to the constitutive model requires the definition of sensitivity coefficients related to the constitutive parameters and temperature, treated as independent variables. The definition of sensitivity coefficients

is done considering a given dependent variable, Y, expressed as a function of independent variables $X_1, \ldots, X_j, \ldots, X_q$

$$Y = G(X_1, \ldots, X_j, \ldots, X_q). \tag{3.12}$$

From the Taylor series expansion, it is possible to write:

$$\delta Y = \left(\frac{\partial G}{\partial X_1}\right) dX_1 + \cdots + \left(\frac{\partial G}{\partial X_j}\right) dX_j + \cdots \left(\frac{\partial G}{\partial X_q}\right) dX_q, \tag{3.13}$$

where $C_j = (\frac{\partial G}{\partial x_j})$ are the sensitivity coefficients. The variance of Y is given by:

$$u^2(Y) = \sum_{j=1}^{q} C_j^2 u^2(X_j). \tag{3.14}$$

The uncertainty of type B, U^V, is the square root of the sum of the contribution of each independent variable multiplied by the student distribution factor. This contribution is evaluated by the variance of each independent variable multiplied by the sensitivity coefficient:

$$U^V = J\sqrt{\sum_{j=1}^{q} C_j^2 u^2(X_j)}, \tag{3.15}$$

where q is the number of independent variables; the independent variable variance is given by

$$u^2(X_j) = a_j^2 \frac{n_{dj}}{k_a n_{rj}}. \tag{3.16}$$

The value of k_a depends on the distribution forms. It assumes values 2, 3 and 6 corresponding to U-shape, triangular or uniform distribution, respectively [Barbato *et al.*, 2005]. The value of n_{dj} corresponds to the input number of the magnitude and n_{rj} is the number of operators that measures this magnitude; a_j is the variation of independent variables for different adjustments divided by 2.

The total uncertainty, U^T, is defined as combination of all uncertainties. Here, it represents a sum of uncertainty due the number of cycles, U^C, and sensitivity coefficients, U^V.

$$U^T = U^c + U^V, \tag{3.17}$$

where U^C is calculated from Eq. (3.4).

The relative uncertainty is defined as the relation between the total uncertainty and the dependent variable:

$$U^R = \frac{U^T}{Y}. \tag{3.18}$$

3.2. *Filtering*

The first step on the uncertainty analysis is to establish a filtering process of the experimental data. Hence, consider the SMA wire experimental tensile tests.

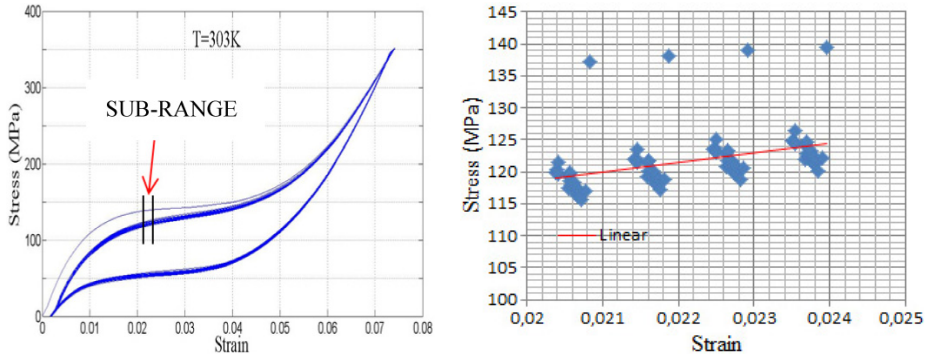

(a) (b)

Fig. 6. Experimental tensile tests. (a) Stress–strain curve for 20 cycles. (b) Zoom related to the strain range (0.02, 0.025), specific region used as example.

The hysteresis curve is divided into 2960 sub-ranges, being 1480 on the upper plateau of the hysteresis loop, associated with the austenite–martensite phase transformation, and 1480 on the lower plateau, associated with the martensite–austenite phase transformation. The strain sub-range (0.02, 0.025) is used to explain the procedure. Figure 6 shows 20 cycles of the stress–strain curve and also a zoom of the specific range.

Linear regression is carried out assuming that $y = ax + b$, where a and b are the adjusted coefficients. First-order residues are calculated from this regression. Figure 7 shows the first-order residue as a function of strain, indicating the trend. Table 2 presents the data corresponding to the linear adjustments and the calculations associated with the standard deviation of the coefficients a and b. In addition, the coefficient of determination ($\mathbb{R}^2$), the standard deviation of the first-order

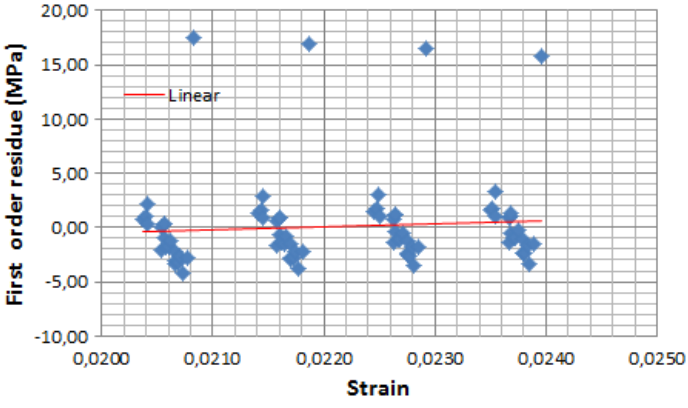

Fig. 7. First-order residue-strain of the range (0.02, 0.025).

Table 2. Statistical data provided by a linear regression for the strain sub-range (0.02, 0.025).

	b	*a*
Coefficients	1258.67	93.63
Standard deviations of the coefficients	265.04	6.02
Robustness	2.39	7.84
Standard deviation of the residues of the first-order	3.87	
Number of degrees of freedom	97.00	
$\mathbb{R}^2$	0.19	

Table 3. First-order residue value.

0.725	−1.734	−2.745	0.838	−2.155	−1.395	−2.543	3.251	−1.128	1.607	−1.088
1.049	−1.752	**17.442**	−0.606	−3.800	1.173	−2.633	0.864	−2.332	3.178	−0.443
2.224	−1.273	1.345	−1.349	−2.203	1.110	−1.835	−1.436	−2.332	0.857	−1.089
0.367	−2.193	1.602	−1.463	**16.968**	−0.397	−3.505	1.073	−2.399	0.854	−2.559
0.072	−3.080	2.880	−0.778	1.520	−1.076	−1.740	1.259	−1.617	−1.483	−2.342
−2.030	−3.291	0.915	−1.574	1.750	−1.150	**16.445**	−0.503	−3.429	1.129	−2.551
0.272	−3.200	−1.630	−2.774	3.066	−0.543	1.582	−0.993	−1.543	−0.608	−1.656
0.327	−2.645	0.652	−2.896	1.048	−1.202	1.687	−0.969	**15.720**	1.061	−3.467
−0.972	−4.178	0.950	−2.798	0.737	−2.345	1.089	−0.256	1.495	−0.935	−1.544

residues, s^{r^1}, the number of degrees of freedom and the robustness are also presented in the Table 2.

The outlier detection and exclusion are done applying Chauvenet's criterion over the values of the first-order residues, presented in Table 3. The values 17.705, 16.629, 15.982 and 15.16 are eliminated for this analysis.

After detecting and excluding all the outliers, the analysis is repeated, evaluating the first-order residues. Figure 8 and Table 4 present the new results. Results of Fig. 8 show the elimination of the systematic errors associated with results of Fig. 7. Linear tendency of the first-order residues is observed.

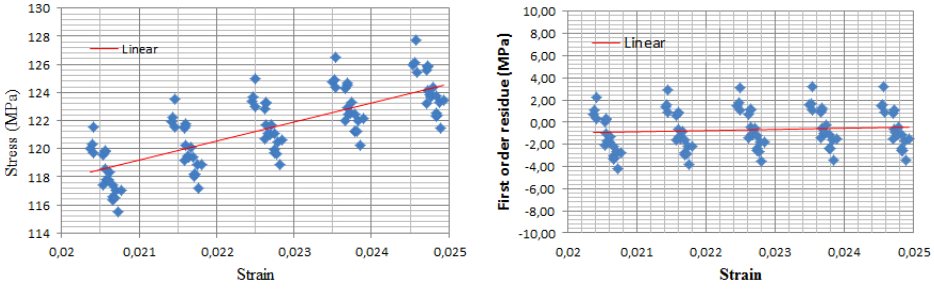

(a) (b)

Fig. 8. Analysis of the strain range (0.02, 0.025). (a) Stress–strain curve. (b) First-order residue-strain curve.

Table 4. Statistical data provided by the linear projection function.

	b	a
Coefficients	1359.82	90.63
Standard deviations of the coefficients	123.55	2.81
Robustness	5.54	16.26
Standard deviation of the residues of the first-order	121.14	
Number of degrees of freedom	93.00	
$\mathbb{R}^2$	0.57	

Table 5. Normal distribution data.

Confidence level	80%
Number of classes	14
Number of constraints	3
Degrees of freedom [d.o.f]	11
Lower boundary of χ^2	5.58
Upper boundary of χ^2	17.28
Experimental χ^2	12.38

Table 4 is used to verify the regression model. Note that the robustness value is greater than 1 indicating that the linear regression is appropriate to represent the experimental data. The coefficient of determination ($\mathbb{R}$) is another important factor to be analyzed indicating how the data is dispersed around the model. For values greater than 0.7 the model represents the data in an appropriate form. Table 5 shows that the experimental Pearson coefficient of correlation (χ^2) defining the lower and upper boundaries of the theoretical values. Figure 9 represents the normal distribution of the residues considering the analysis before and after the outlier detection and exclusion. Note that the procedure brings the experimental distribution closer to a normal distribution.

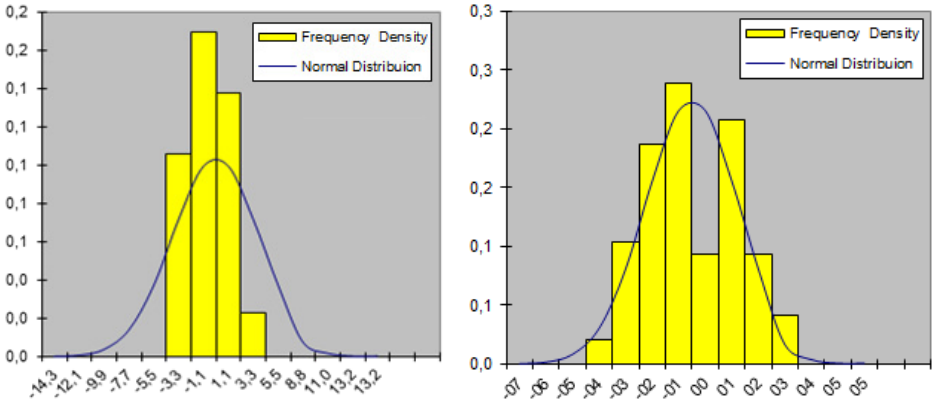

(a) (b)

Fig. 9. Effect of outlier detection and exclusion of systematic errors. (a) Before the analysis. (b) After the analysis.

This analysis identifies that the first of the 20 cycles is an outlier. Therefore, it is neglected and all the analysis considers just the subsequent 19 cycles.

4. Constitutive Model

The thermomechanical description of SMAs is very complex, being the objective of several research efforts. Lagoudas [2008] and Paiva and Savi [2006] presented a general overview of the constitutive models employed for this aim. This work employs the model with internal constraints proposed by Paiva *et al.* [2005], and discussed in the following references: Savi *et al.* [2002], Baêta-Neves *et al.* [2004], Savi and Paiva [2005] and Monteiro *et al.* [2009]. This 1D macroscopic model considers different material properties for each phase. It includes four macroscopic phases: three variants of martensite (M^+, M^-, M) and an austenitic (A) phase. M^+ and M^- are detwinned martensites, which are induced by stress fields and M is twinned martensite, which is stable in low temperatures, in the absence of a stress field. For the sake of simplicity, this work does not take into account tension–compression asymmetry, the plasticity and the transformation induced by plasticity, considered in the previous versions of the model. In addition, only tensile martensite is of concern in order to reproduce the experimental tests. Under these assumptions, it is possible to highlight the most important effects and the uncertainty influences.

The constitutive equations are defined from state variables that include strain, ε, and temperature, T. Besides, two volume fractions are considered: β^+ is associated with tensile detwinned martensite (M+) and β^A represents austenite (A). Twinned martensite M can be obtained from the phase coexistence argument: $\beta^M = 1 - \beta^+ - \beta^A$. The set of constitutive equations is presented in the sequence:

$$\sigma = E\varepsilon - (E\alpha^h + \alpha)\beta^+ - \Omega(T - T_0) \tag{4.1}$$

$$\dot{\beta}^+ = \frac{1}{\eta^+} + \{\alpha\varepsilon + \Lambda^+ - (2\alpha^h\alpha + E(\alpha^h)^2)\beta^+ + \alpha^h(E\varepsilon - \Omega(T - T_0)) - \tau^+\} + \tau^+, \tag{4.2}$$

$$\dot{\beta}^A = \frac{1}{\eta^A}\left\{\frac{1}{2}(E^A - E^M)(\varepsilon + \alpha^h\beta^+)^2 + \Lambda^A + (\Omega^A - \Omega^M)(T - T_0)(\varepsilon + \alpha^h\beta^+) - \tau^A\right\} + \tau^{\mathbf{A}}. \tag{4.3}$$

In these equations, the following terms are related to projections that assure a proper coexistence of the involved phases.

$$\tau = [\tau^+, \tau^A] \in \partial I_\pi(\beta^+, \beta^A), \tag{4.4}$$

$$\tau = [\tau^+, \tau^A] \in \partial I_\chi(\dot{\beta}^+, \dot{\beta}^A). \tag{4.5}$$

These projections are defined from the sub-differential of the indicator functions related to internal constraints. The indicator function $I_\pi(\beta^+, \beta^A)$ is related to the

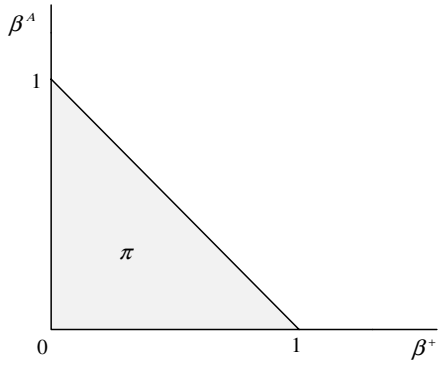

Fig. 10. Geometrical representation of the phase's coexistence restriction.

convex set that can be geometrically interpreted by a triangle in β^+, β^A – space, shown in Fig. 10.

$$\pi = \{\beta^m \in \Re \,|\, 0 \leq \beta^m \leq 1 (m = +, A); \beta^+ + \beta^A \leq 1\}. \tag{4.6}$$

Moreover, I_χ is the indicator function related to the convex set χ, which provides constraints associated with phase transformation evolution, such as internal subloops due to incomplete phase transformation description [Savi and Paiva, 2005].

In the previous equations, subscript M is related to the martensitic phase while A is associated with austenite; α is the parameter related to the vertical size of the stress–strain hysteresis loop, α^h is the parameter related to the horizontal size of the stress–strain hysteresis loop while Λ's are associated with phase transformations stress levels; E's represent the elastic modulus, Ω's are related to the thermal expansion coefficients; T_0 is a reference temperature; and $\eta^m (m = +, A)$ are associated with the internal dissipation of each material phase. Furthermore, the parameters E and Ω are defined from their austenitic and martensitic phase values:

$$E = E^M + \beta^A [E^M - E^A], \tag{4.7}$$

$$\Omega = \Omega^M + \beta^A [\Omega^M - \Omega^A], \tag{4.8}$$

while Λ^+ and Λ^A are temperature dependent being defined as follows:

$$\Lambda^+ = \begin{cases} -L_0^+ + \dfrac{L^+}{T^M}(T - T^M), & \text{if } T > T^M \\ -L_0^+, & \text{if } T \leq T^M \end{cases} \tag{4.9}$$

$$\Lambda^A = \begin{cases} -L_0^A + \dfrac{L^A}{T^M}(T - T^M), & \text{if } T > T^M \\ -L_0^A, & \text{if } T \leq T^M \end{cases} \tag{4.10}$$

Table 6. Constitutive parameters.

E^A (GPa)	E^M (GPa)	Ω^A (MPa/K)	Ω^M (MPa/K)	α (MPa)	α^h
9.9	9.9	0.74	0.17	100	0.0365
L_0^+ (MPa)	L^+ (MPa)	L_0^A (MPa)	L^A (MPa)	η^+ (MPa.s)	η^A (MPa.s)
0.01	74	1	108	2	2
T^M (K)	T_0 (K)				
270.12	307				

where T^M is the temperature below which the martensitic phase becomes stable in a stress-free state. In addition, L_0^+, L_0^+, L_0^A and L^A are parameters related to phase transformation critical stresses.

Table 6 shows constitutive parameters employed to match experimental tests. Note that model parameters are related to thermoelastic and phase transformation properties.

5. Uncertainty Estimation

The uncertainty associated with constitutive model is estimated by considering that the stress σ is the dependent variable, while constitutive parameters, $E^M, E^A, \Omega^M, \Omega^A, \alpha^h, \alpha, L_0^+, L^+, L_0^A, L^A, \eta^+, \eta^A$ and T^M and the temperature, T, are independent variables.

Appendix A presents the sensitivity coefficients C_j calculated with respect to dependent variables. This calculation considers a discretized version of the constitutive equations, as follows:

$$\sigma_n = E\varepsilon_n - (E\alpha^h + \alpha)\beta_n^+ - \Omega(T_n - T_0) \tag{5.1}$$

$$\beta_n^+ = \beta_{n-1}^+ + \left\{ \frac{1}{\eta^+}[\alpha E + \Lambda^+ - (2\alpha^h\alpha + E(\alpha^h)^2)\beta_n^+ + \alpha^h(E\varepsilon_n - \Omega(T_n - T_0)) - \tau^+] + \tau^+ \right\} \Delta t, \tag{5.2}$$

$$\beta_n^A = \beta_{n-1}^A + \left\{ \frac{1}{\eta^A} \left[\frac{1}{2}(E^A - E^M)(\varepsilon_n - \alpha^h\beta_n^+)^2 + \Lambda^A + (\Omega^A - \Omega^M)(T_n - T_0)(\varepsilon_n - \alpha^h\beta_n^+) - \tau^A \right] + \tau^A \right\} \Delta t, \tag{5.3}$$

where subscripts n and $n-1$ define the actual and previous time step.

The contribution of each uncertainty is calculated by dividing the hysteresis curve into 592 parts, being 296 on the upper plateau, associated with the austenite–martensite phase transformation, and 296 on the lower plateau, associated with the martensite–austenite phase transformation. Besides, each of these parts is divided

into sub-ranges as in the previous analysis. Basically, it is assumed ranges of 0.0025 and each sub-range is divided into four equal parts.

5.1. *Uncertainty related to the number of cycles*

This section is dedicated to evaluate uncertainty contribution related to the number of cycles to which SMA specimen is subjected. Basically, experimental tests consider 20 cycles, but the first one is discarded by the application of the outlier process. Afterward, an average value concerning the stress and strain of all 19 cycles inside each sub-range of 0.000625 is calculated with their respective number of points, called $\bar{m}^{\sigma}$ and $\bar{m}^{\varepsilon}$, respectively. The standard deviations, $\bar{s}^{\sigma}$, is then calculated. Finally, the average of the standard deviation of the stress, the average of stress and strain from each interval of 0.0025, s^{σ}, m^{σ} and m^{ε} respectively, are calculated from the average of four values of $\bar{s}^{\sigma}, \bar{m}^{\sigma}$ and $\bar{m}^{\varepsilon}$ for each interval.

$$s^{\sigma} = \frac{\sum_{i=1}^{4} \bar{s}^{\sigma}}{4}, \tag{5.4}$$

$$m^{\sigma} = \frac{\sum_{i=1}^{4} \bar{m}^{\sigma}}{4}, \tag{5.5}$$

$$m^{\varepsilon} = \frac{\sum_{i=1}^{4} \bar{m}^{\varepsilon}}{4}. \tag{5.6}$$

From Eq. (3.4), it is possible to calculate the value of the uncertainty related to the number of cycles, $U^{c} = Js^{\sigma}$, where the student factor, J, is assumed to be 2 for a confidence level of 95%.

Figure 11(a) presents a comparison between numerical simulations and experimental data expressed as the average stress, m^{σ}, and the average strain, m^{ε}. Besides,

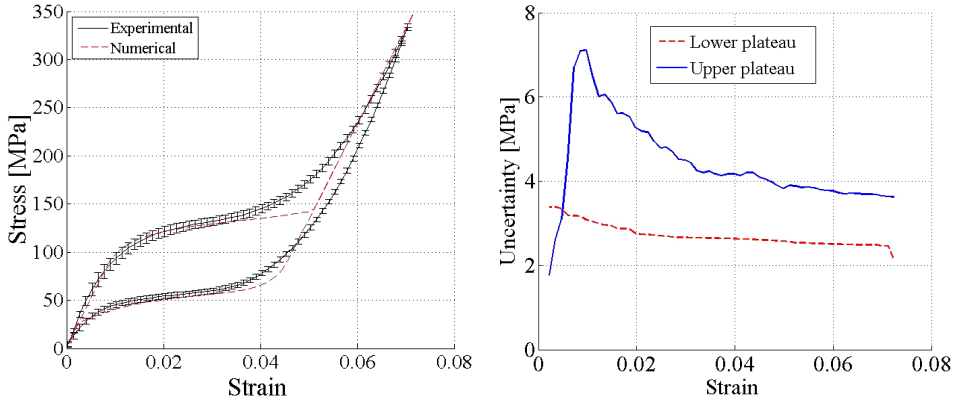

(a) (b)

Fig. 11. Uncertainty analysis due to the number of cycles. (a) Stress–strain curve. (b) Comparison between upper and lower plateaus uncertainties.

a range represented by bars with the uncertainty contribution values, U^c, defines experimental results. Figure 11(b) shows the comparison between the uncertainty of the upper and the lower plateaus of the hysteresis loop. Note that the uncertainty contribution of the upper plateau is greater than the one of the lower plateau. Moreover, it is important to observe that the uncertainty is relevant. It is important to highlight that, in general, the model in within the range of uncertainty of the experimental data. The exceptions are the regions related to the finish of the austenite–martensite transformation and also the region of the start of the reverse transformation.

5.2. *Uncertainty related to the independent variables (type B)*

Sensitivity coefficients related to independent variables are now in focus. The coefficients a_j are calculated using constitutive parameters presented in Table 6 as reference values. The calculation considers perturbations from each independent variable separately, performing a new adjustment with the perturbed value. A comparison between both stress–strain curves defines a perturbation responsible for the variation. The magnitude of the difference between the reference value and the perturbed value of the independent variable, divided by 2, is the value of a_j for the respective independent variable. The following parameters are assumed for uncertainty analysis: $k_a = 3$ (uniform distribution); $n_{dj} = 1$ (single input); $n_{rj} = 1$ (single output).

Figure 12 shows the comparison between numerical simulations and experimental data with uncertainty contributions. Figure 12(a) shows stress–strain curve related to both numerical simulation and experimental data together with bars representing the contribution of uncertainty U^V. Figure 12(b) shows the comparison between the uncertainties related to lower and upper plateaus of the hysteresis loop.

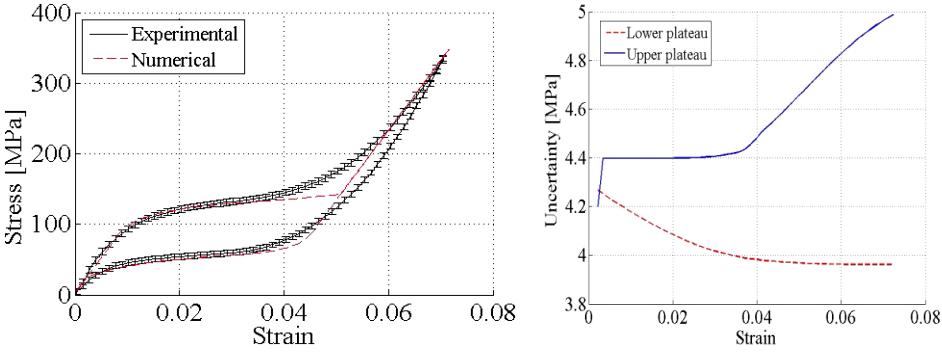

(a) (b)

Fig. 12. Uncertainty analysis due to the sensitivity coefficients. (a) Stress–strain curve. (b) Comparison between upper and lower uncertainty.

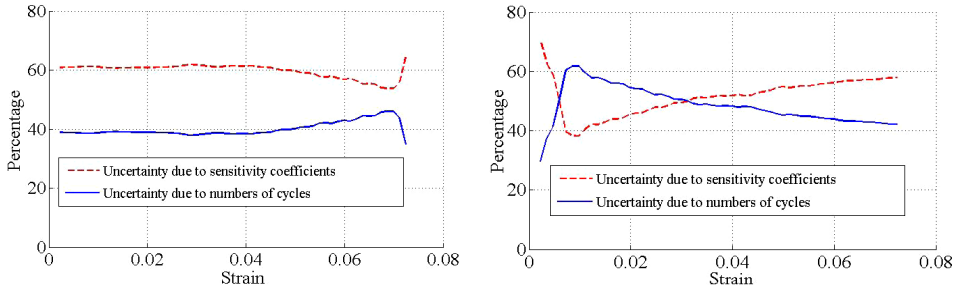

Fig. 13. Effects of uncertainty due to the number of cycles and parameters variations. (a) Lower plateau of the hysteresis loop. (b) Upper plateau of the hysteresis loop.

By establishing a comparison between uncertainties related to independent variables, U^V, and associated with the number of cycles, U^c, it is noticeable that the first one is less expressive than the second one with respect to the upper plateau of the hysteresis loop, for low strain values. On the other hand, the lower plateau presents a greater contribution of the uncertainty U^V than the one of the uncertainty U^c. This comparison is shown in Fig. 13. Note that the sensitivity coefficients have greater impact on the total uncertainty value on the lower plateau of the hysteresis loop. On the upper plateau, the sensitivity coefficients and the number of cycles have different impact during the process. Nevertheless, it should be pointed out that the uncertainty due to variations of the independent variables and the number of cycles vary during mechanical loading imposed on the specimen.

Figure 14 presents the relative uncertainty as a function of strain. Note that this contribution is more important for small strain values. This behavior is mainly due to the contribution of the uncertainty due to the number of cycles.

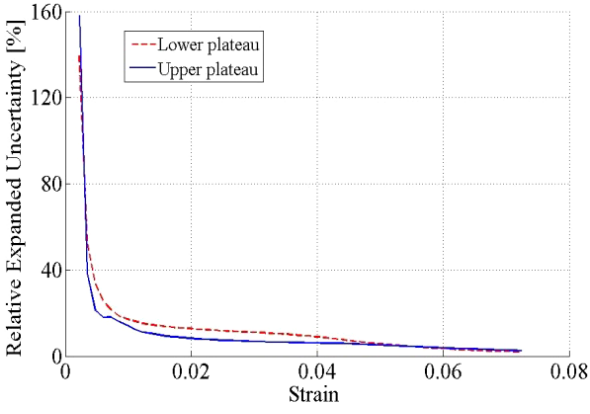

Fig. 14. Relative expanded uncertainty (U^R).

Concerning dependent variables, constitutive parameters, E^A and E^M, and temperature, T, has the most important contributions to uncertainty. Figure 15 shows the percentage variation of each one of these variables with respect to the total uncertainty.

The contribution of the total uncertainty, U^T, defined by a combination of uncertainties due the number of cycles and sensitivity coefficients, is now in focus. Figure 16 shows the comparison between numerical simulations and experimental data with uncertainty contributions. It is important to observe that numerical simulations are inside the acceptable region defined by uncertainties. Nevertheless, it

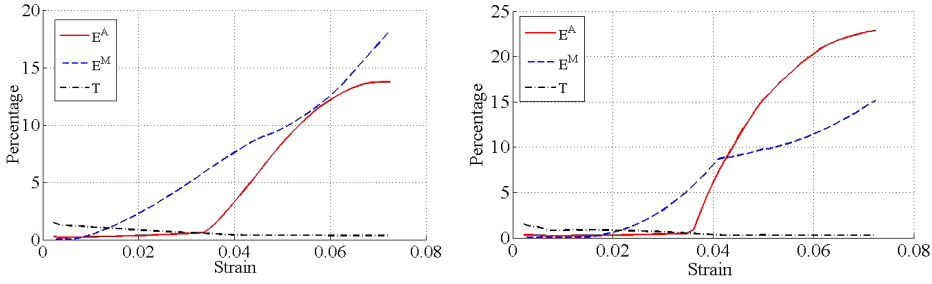

Fig. 15. Sensitivity coefficient influence with respect to the total uncertainty. (a) Lower plateau of the hysteresis loop. (b) Upper plateau of the hysteresis loop.

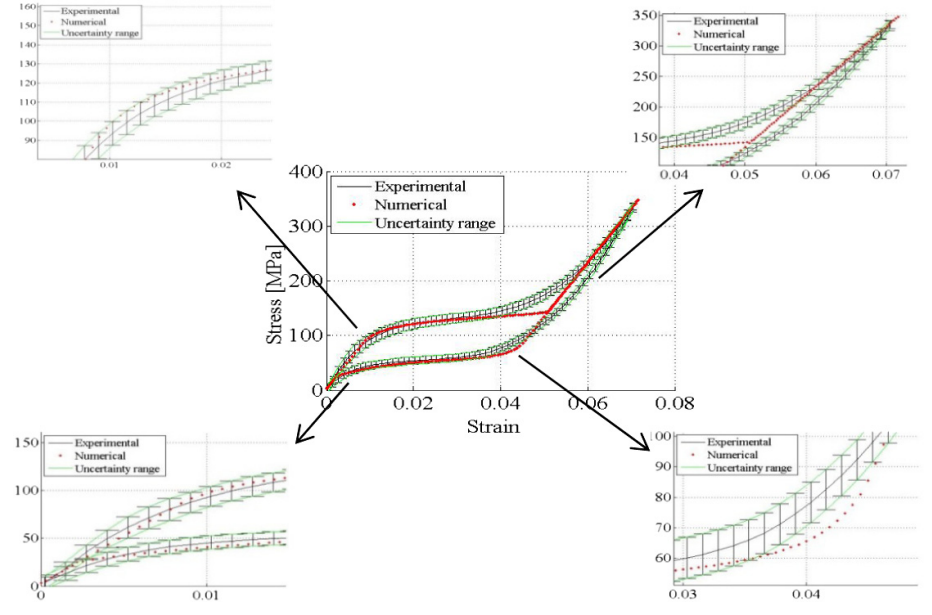

Fig. 16. Comparison between numerical and experimental results of the stress–strain curve considering total uncertainty contribution.

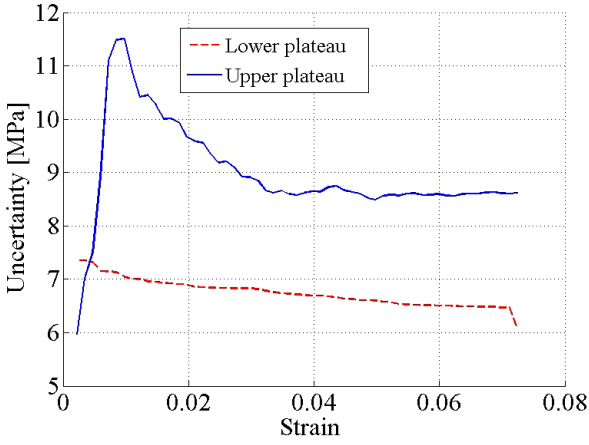

Fig. 17. Comparison between total uncertainties related to upper and lower plateaus of the hysteresis loop.

should be observed that there are four critical regions, related to start and finish of phase transformations. These regions are highlighted in Fig. 16. The region of the finish of austenite–martensite is especially critical since experimental data defines a region around linear elastic response. This critical situation has an influence on the start of the reverse transformation, from martensite to austenite. Figure 17 presents the uncertainty contributions related to the upper and lower plateaus of the hysteresis loop. The upper plateau has a more significant importance, exactly due to the mentioned critical region.

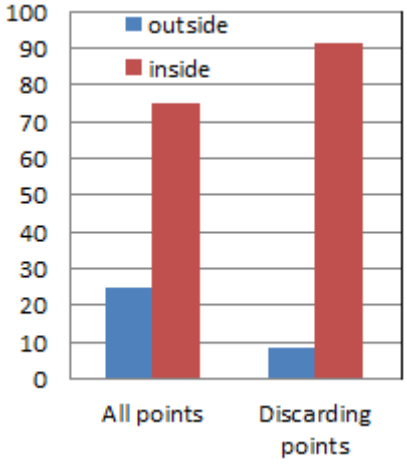

Fig. 18. Comparison of the numerical simulation points that are inside and outside the uncertainty range of the experimental data.

Figure 18 represents the model ability to reproduce experimental data. It presents the distribution of the numbers of points inside and outside the uncertainty range. Note that 76.09% of the numerical results are inside the range while 23.91% are outside. If the critical region of the finish of austenite–martensite phase transformation is discarded, these numbers change to 91.62% inside and 8.38% outside the uncertainty range. This result can be considered a close agreement since it captures the general, strong nonlinear thermomechanical behavior of SMAs.

6. Conclusions

This paper deals with the uncertainty analysis of the thermomechanical description of SMAs. Experimental data obtained from tensile tests are treated together with numerical simulations associated with a constitutive model proposed by Paiva *et al.* [2005]. Two uncertainty contributions are investigated: due to the number of cycles; and due to constitutive parameters. Concerning sensitivity coefficients, the constitutive parameters that present the greater influence with respect to uncertainty are the elastic moduli, E^A and E^M. Besides, temperature has also an important contribution. Results show that numerical simulations are inside the uncertainty range of the experimental data. Regions associated with the finish of austenite–martensite phase transformation and start of martensite–austenite transformation present some discrepancies. Nevertheless, the model is capable to capture the general aspects of experimental data fitting the strong nonlinear thermomechanical behavior of SMAs. This analysis should be considered as an essential verification of the constitutive model, encouraging its use in SMA description. Different phenomena related to SMA thermomechanical behavior and also more sophisticated analyses including 3D media can be developed from the results of this uncertainty analysis.

Acknowledgments

The authors would like to acknowledge the support of the Brazilian Research Agencies CNPq, CAPES and FAPERJ and through the INCT-EIE (National Institute of Science and Technology — Smart Structures in Engineering) the CNPq and FAPEMIG. The Air Force Office of Scientific Research (AFOSR) is also acknowledged. In addition, the authors express their gratitude to Professor Giulio Barbato *et al.* (Politecnico di Torino, Dipartamento di Ingegneria Gestionale e della Produzione) for all his insightful comments.

Appendix

This appendix presents the sensitivity coefficients calculated for each independent variable of the constitutive model.

Definition of auxiliary variables

$$\gamma = \left(\varepsilon - \alpha^h \left(\beta_{n-1}^+ + \frac{\Delta t(\alpha\epsilon + \Lambda^+ - \beta^+(2\alpha^h\alpha + \alpha^h E) + \alpha^h[\epsilon E - \Omega(T - T_0))}{\eta^+}\right)\right),$$

$$\mathcal{L} = \left(E^M - (E^M - E^A)\left(\begin{matrix}(\Lambda^A + 0.5(-\alpha^h\beta^+ + \epsilon)^2(E^A - E^M) \\ \beta_{n-1}^A + \frac{+(-\alpha^h\beta^+ + \epsilon)(\Omega^A - \Omega^M)(T - T_0))}{\eta^A}\end{matrix}\right)\right),$$

$$\psi = \frac{(\Lambda^A + 0.5(-\alpha^h\beta^+ + \epsilon)^2(E^A - E^M) + (-\alpha^h\beta^+ + \epsilon)(\Omega^A - \Omega^M)(T - T_0))\Delta t}{\eta^A}$$

(a) *E^M Sensitivity Coefficient*

$$\begin{aligned} C_{E^M} = &-\frac{\alpha(-\alpha^h\beta^+(1-\beta^A) + \alpha^h\varepsilon(1-\beta^A))\Delta t}{\eta^+} \\ &+\gamma\left(1 + \frac{0.5(-\alpha^h\beta^+ + \epsilon)^2(E^M - E^A)\Delta t}{\eta^A} - \beta_{n-1}^A - \psi\right) \\ &-\mathcal{L}\left(\frac{(\alpha^h)^2(1-\beta^A)(-\beta^+ + \epsilon)\Delta t}{\eta^+}\right) \\ &-\frac{0.5(-\alpha^h\beta^+ + \epsilon)^2(\Omega^M - \Omega^A)(T - T_0)\Delta t}{\eta^A} \end{aligned}$$

(b) *E^A Sensitivity Coefficient*

$$\begin{aligned} C_{E^A} = &-\frac{\alpha(-\alpha^h\beta^+\beta^A + \alpha^h\varepsilon\beta^A)\Delta t}{\eta^+} \\ &+\gamma\left(-\frac{(0.5(-\alpha^h\beta^+ + \epsilon)^2(E^M - E^A))\Delta t}{\eta^A} + \beta_{n-1}^A + \psi\right) \\ &-\mathcal{L}\left(\frac{(\alpha^h)^2\beta^A(-\beta^+ + \epsilon)\Delta t}{\eta^+}\right) \\ &+\frac{0.5(-\alpha^h\beta^+ + \epsilon)^2(\Omega^M - \Omega^A)(T - T_0)\Delta t}{\eta^A}. \end{aligned}$$

(c) *Ω^A Sensitivity Coefficient*

$$\begin{aligned} C_{\Omega^A} = &\mathcal{L}\left(\frac{(\alpha^h)^2\beta^A(T - T_o)\Delta t}{\eta^+}\right) + \frac{\alpha\alpha^h\beta^A(T - T_o)\Delta t}{\eta^+} \\ &-\gamma\left(\frac{(-\alpha^h\beta^+ + \epsilon)(E^A - E^M)\Delta t}{\eta^A}\right)(T - T_0) \\ &-\left((\beta_{n-1}^A + \psi) - \frac{(-\alpha^h\beta^+ + \epsilon)(\Omega^M - \Omega^A)(T - T_0)\Delta t}{\eta^A}\right)(T - T_0) \end{aligned}$$

(d) Ω^M *Sensitivity Coefficient*

$$C_{\Omega}^{M} = \mathcal{L}\left(\frac{(\alpha^h)^2(1-\beta^A)(T-T_0)\Delta t}{\eta^+}\right) + \frac{\alpha\alpha^h(1-\beta^A)(T-T_0)\Delta t}{\eta^+}$$
$$+\gamma\left(\frac{(-\alpha^h\beta^+ + \epsilon)(E^A - E^M)\Delta t}{\eta^A}\right)(T-T_0)$$
$$-\left((1-\beta_{n-1}^A - \psi) + \frac{(-\alpha^h\beta^+ + \epsilon)(\Omega^M - \Omega^A)(T-T_0)\Delta t}{\eta^A}\right)(T-T_0)$$

(e) α^h *Sensitivity Coefficient*

$$C_{\alpha^h} = \mathcal{L}\left(-\beta_{n-1}^+ - \frac{(\alpha\epsilon + \Lambda^+ - \beta^+(2\alpha\alpha^h + \alpha^h E) + \alpha^h[\epsilon E - \Omega(T-T_o))\Delta t}{\eta^+}\right.$$
$$\left. - \frac{\alpha^h(\varepsilon E - \beta^+(2\alpha + E) - \Omega(T-T_0))\Delta t}{\eta^+}\right)$$
$$-\gamma\left(\frac{-E^A + E^M}{\eta^A}\right)\Delta t(-\beta^+(-\alpha^h\beta^+ + \epsilon)(E^A - E^M)$$
$$-\beta^+(\Omega^A - \Omega^M)(T-T_o))$$
$$-\frac{\alpha(\varepsilon E - \beta^+(2\alpha + E) - \Omega(T-T_0))\Delta t}{\eta^+}$$
$$+\frac{-(\Omega^A - \Omega^M)(T-T_o)(-\beta^+(-\alpha^h\beta^+ + \epsilon)(E^A - E^M) - \beta^+(\Omega^A - \Omega^M)(T-T_0)\Delta t)}{\eta^A}$$

(f) α *Sensitivity Coefficient*

$$C_{\alpha} = -\frac{\alpha(-2\alpha^h\beta^+ + \epsilon)\Delta t}{\eta^+} - \beta_{n-1}^+ - \mathcal{L}\left(\frac{\alpha^h(-2\alpha^h\beta^+ + \epsilon)\Delta t}{\eta^+}\right)$$
$$-(\alpha\epsilon + \Lambda^+ - \beta^+(2\alpha\alpha^h + \alpha^h E) + \frac{\alpha^h(\epsilon E - \Omega(T-T_0))\Delta t}{\eta^+}$$

(g) η^+ *Sensitivity Coefficient*

$$C_{\eta^+} = \frac{\alpha\Delta t(\alpha\epsilon + \Lambda^+ - \beta^+(2\alpha\alpha^h + \alpha^h E) + \alpha^h[\epsilon E - \Omega(T-T_0))}{(\eta^+)^2}$$
$$+\frac{\alpha^h\Delta t}{(\eta^+)^2}\mathcal{L}(\alpha\epsilon + \Lambda^+ - \beta^+(2\alpha\alpha^h + \alpha^h E) + \alpha^h[\epsilon E - \Omega(T-T_0))$$

(h) C_{η^A} *Sensitivity Coefficient*

$$C_{\eta^A} = \frac{(E^M - E^A)\Delta t}{(\eta^A)^2}\gamma(\Lambda^A + 0.5(-\alpha^h\beta^+ + \epsilon)^2(E^A - E^M)$$
$$+(-\alpha^h\beta^+ + \epsilon)(\Omega^A - \Omega^M)(T-T_0)) - \frac{(\Omega^M - \Omega^A)(T-T_0)}{\eta^A}\psi$$

(i) L_0^+ *Sensitivity Coefficient*

$$C_{L_0^+} = \frac{\alpha \Delta t}{\eta^+} + \frac{\alpha^h \mathcal{L} \Delta t}{\eta^+}$$

(j) L_0^A *Sensitivity Coefficient*

$$C_{L_0^A} = \frac{\gamma (E^M - E^A) \Delta t}{\eta^A} - \frac{(\Omega^M - \Omega^A)(T - T_0) \Delta t}{\eta^A}$$

(k) L^+ *Sensitivity Coefficient*

$$C_{L^+} = -\frac{\alpha (T - T^M) \Delta t}{\eta^+ T^M} - \frac{\alpha^h (T - T^M) \mathcal{L} \Delta t}{\eta^+ T^M}$$

(l) L^A *Sensitivity Coefficient*

$$L^A = \frac{(E^A - E^M)(T - T^M) \gamma \Delta t}{\eta^A T^M} - \frac{(\Omega^A - \Omega^M)(T - T_o)(T - T^M) \Delta t}{\eta^A T^M}$$

(m) T^M *Sensitivity Coefficient*

$$\begin{aligned} C_{T^M} = & \frac{\alpha (\frac{L^+ (T - T^M)}{(T^M)^2} + \frac{L^+}{T^M}) \Delta t}{\eta^+} + \gamma \frac{(E^M - E^A)(\frac{L^A (T - T^M)}{(T^M)^2} + \frac{L^A}{T^M}) \Delta t}{\eta^A} \\ & + \mathcal{L} \frac{\alpha^h (\frac{L^+ (T - T^M)}{(T^M)^2} + \frac{L^+}{T^M}) \Delta t}{\eta^+} \\ & - \frac{(\Omega^M - \Omega^A)(T - T_0)(\frac{L^A (T - T^M)}{(T^M)^2} + \frac{L^A}{T^M}) \Delta t}{\eta^A} \end{aligned}$$

(n) T *Sensitivity Coefficient*

$$\begin{aligned} C_T = & -\Omega^M - \frac{\alpha \Delta t (\alpha^h \Omega + \frac{L^+}{T^M})}{\eta^+} \\ & - \gamma \frac{(E^M - E^A)((-\alpha^h \beta^+ + \epsilon)(\Omega^A - \Omega^M) - \frac{L^A}{T^M}) \Delta t}{\eta^A} - \mathcal{L} \frac{\alpha^h \Delta t (\alpha^h \Omega + \frac{L^+}{T^M})}{\eta^+} \\ & - (\Omega^A - \Omega^M)(\beta_{n-1}^A + \psi) \\ & + \frac{(\Omega^M - \Omega^A)(T - T_o)((-\alpha^h \beta^+ + \epsilon)(\Omega^A - \Omega^M) - \frac{L^A}{T^M}) \Delta t}{\eta^A}. \end{aligned}$$

References

Aguiar, R. A. A., Savi, M. A. and Pacheco, P. M. C. L. [2010] " Experimental and numerical investigations of shape memory alloy helical springs," *Smart Materials and Structures* **19**(2), 025008.

Andani, M. T., Alipour, A. and Elahinia, M. [2013] "Coupled rate-dependent superelastic behavior of shape memory alloy bars induced by combined axial-torsional loading: A semi-analytic modeling," *Journal of Intelligent Material Systems and Structures* **24**(16), 1995–2007.

Andani, M. T. and Elahinia, M. [2014] "A rate dependent tension–torsion constitutive model for superelastic nitinol under non-proportional loading: A departure from von Mises equivalency," *Smart Materials and Structures* **23**, 015012.

Auricchio, F., Bonetti, E., Scalet, G. and Ubertini, F. [2014] "Theoretical and numerical modeling of shape memory alloys accounting for multiple phase transformations and martensite reorientation," *International Journal of Plasticity* **59**, 30–54.

Baêta-Neves, A. P., Savi, M. A. and Pacheco, P. M. C. L. [2004] "On the Fremond's constitutive model for shape memory alloys," *Mechanics Research Communication* **6**(31), 677–688.

Barbato, G., Germak, A. and D'Agostino, D. [2005] "Misurare per decidere," Progetto Leonardo, Bologna.

BIPM, IEC; IFCC, ISO; IUPAC OIML [2008] Evaluation of measurement data guide to the expression of uncertainty in measurement JCGM 100:2008.

Chapman, C., Eshghinejad, A. and Elahinia, M. [2011] "Torsional behavior of NiTi wires and tubes: Modeling and experimentation," *Journal of Intelligent Material Systems and Structures* **22**, 1239–1248.

Coleman, H. W. and Steele, W. G. [1995] "Engineering application of experimental uncertainty analysis," *AIAA Journal* **33**(10), 1888–1896.

Czechowicz, A. [2013] "On the functional characteristics of pseudoelastic adaptive resetting of shape memory actuators in the field of automotive applications," *Journal of Intelligent Material Systems and Structures* **24**(13), 1539–1545.

Fremond, M. [1996] "Shape memory alloy: A thermomechanical macroscopic theory," *CISM Courses and Lectures* **351**, 3–68, New York.

ISO/TS 14253-2, "Geometrical Product Specifications (GPS) [1999] — Inspection by measurement of workpieces and measuring equipment — Part 2: Guide to the estimation of uncertainty in GPS measurement," in calibration of measuring equipment and in product verification.

Lagoudas, D. C. [2008] *Shape Memory Alloys: Modeling and Engineering Applications*, Springer Science Business Media, LLC, New York.

Lagoudas, D. C., Hartl, D., Chemisky, Y., Machado, L. G. and Popov, P. [2011] "Constitutive model for the numerical analysis of phase transformation in polycrystalline shape memory alloys," *International Journal of Plasticity* **32**, 155–183.

Lemaitre, J. and Charboche, J. L. [1990] *Mechanics of Solid Materials*, Cambridge University Press, London.

Machado, L. G. and Savi, M. A. [2003] "Medical applications of shape memory alloys," *Brazilian Journal of Medical and Biological Research* **36**(6), 683–691.

Mehrabi, R. and Kadkhodaei, M. [2013] "3D phenomenological constitutive modeling of shape memory alloys based on microplane theory," *Smart Materials and Structures* **22**, 025017.

Moffat, R. J. [1985] "Using uncertainty analysis in the planning of an experiment," *ASME Transactions, Journal of Fluids Engineering* **107**, 173–178.

Moffat, R. J. [1988] "Describing the uncertainties in experimental results," *Experimental Thermal and Fluid Science* **1**, 3–17.

Monteiro, P. C. C., Savi, M. A., Netto, T. A. and Pacheco, P. M. C. L. [2009] "A phenomenological description of the thermomechanical coupling and the rate-dependent

behavior of shape memory alloys," *Journal of Intelligent Material Systems and Structures* **20**(14), 1675–1687.

Oliveira, S. A., Savi, M. A. and Kalamkarov, A. L. [2010] "A three-dimensional constitutive model for shape memory alloys," *Archive of Applied Mechanics* **80**(10), 1163–1175.

Paiva, A. and Savi, M. A. [2006] "An overview of constitutive models for shape memory alloys," *Mathematical Problems in Engineering*.

Paiva, A., Savi, M. A., Braga, A. M. B. and Pacheco, P. M. C. L. [2005] "A constitutive model for shape memory alloys considering tensile-compressive asymmetry and plasticity," *International Journal of Solids and Structures* **42**(11–12), 3439–3457.

Panico, M. and Brinson, L. C. [2007] "A three-dimensional phenomenological model for martensite reorientation in shape memory alloy," *Journal of the Mechanics and Physics of Solids* **55**(11), 2491–2511.

Savi, M. A. [2014] "Nonlinear dynamics and chaos in shape memory alloy systems," *International Journal of Nonlinear Mechanics*, doi:10.1016/j.ijnonlinmec.2014.06.001.

Savi, M. A., Paiva, A., Baeta-Neves, A. P. and Pacheco, P. M. C. L. [2002] "Phenomenological modeling and numerical simulation of shape memory: A thermo-plastic-phase transformation coupled model," *Journal of Intelligent Materials Systems and Structures* **3**(5), 261–273.

Savi, M. A. and Paiva, A. [2005] "Describing internal subloops due to incomplete phase transformations in shape memory alloys," *Archive of Applied Mechanics* **74**(9), 637–647.

Steele, W. G. and Coleman, H. W. [1987] "Use of uncertainty analysis in the planning and design of an experimental," *American Society of Mechanical Engineering*, *Fluid Mechanics* **58**, 63–67.